

Antagonistic Roles for H3K36me3 and H3K27me3 in the Cold-Induced Epigenetic Switch at *Arabidopsis FLC*

Hongchun Yang,¹ Martin Howard,² and Caroline Dean^{1,*}

¹Department of Cell and Developmental Biology, John Innes Centre, Norwich Research Park, Norwich NR4 7UH, UK

²Computational and Systems Biology, John Innes Centre, Norwich Research Park, Norwich NR4 7UH, UK

Summary

Posttranslational modifications of histone tails are an important factor regulating chromatin structure and gene expression. Epigenetic memory systems have been predicted to involve mutually exclusive histone modifications that, through positive feedback mechanisms, generate bistable states [1, 2]. How the states are interconverted is not understood, and whether the histone modifications are sufficient for epigenetic memory is still greatly debated [3]. We have exploited the process of vernalization, the slow quantitative epigenetic silencing of *Arabidopsis FLC* induced by cold, to detail with fine temporal and spatial resolution the dynamics of histone modifications during an epigenetic switch. The profiles of H3K36me3, H3K4me3, and H3K4me2 at *FLC* throughout the vernalization process were compared to H3K27me3, which accumulates at a local nucleation region during the cold and spreads across the locus on return to the warm [2]. We find for many phases of the vernalization process that H3K36me3 and H3K27me3 show opposing profiles in the *FLC* nucleation region and gene body, that H3K36me3 and H3K27me3 rarely coexist on the same histone tail, and that this antagonism is functionally important. A lack of H3K36me3 results in a fully silenced state at *FLC* even in the absence of cold. We therefore propose that H3K36me3 is the opposing modification to H3K27me3 in the Polycomb-mediated silencing of *FLC*. However, the lack of an absolute mirror profile predicted from modeling suggests that their antagonistic roles contribute a necessary, but not sufficient, component of the mechanism enabling switching between and inheritance of epigenetic states.

Results and Discussion

Previously, we developed a mathematical model aimed at explaining the quantitative basis of the epigenetic silencing of *FLC* during vernalization [2]. The model incorporates a highly dynamic chromatin environment in which opposing histone modifications are constantly being added and removed. Through implicit recruitment of appropriate protein complexes, one type of histone modification can promote both the addition of further modifications of the same type and removal of modifications of the opposing type. Such positive-feedback mechanisms can result in either of the antagonistic histone modifications becoming self-sustaining, leading

to opposing epigenetically stable states [1, 2, 4, 5]. For *FLC*, we envisioned an actively transcribed “A” state that switches to a stably repressed “M” state during vernalization. Genetic and chromatin immunoprecipitation (ChIP) analysis had shown that Polycomb activity, which induces H3K27me3 modifications, was consistent with the M state at *FLC* [2, 6–8]. The targeted nucleation of a modified Polycomb complex—PHD-PRC2—at a localized “nucleation” region within *FLC*, enabled switching of *FLC* to an epigenetically stable silent expression state [2, 6–9]. This switch was associated with spreading of the PHD-PRC2 complex and enhanced H3K27me3 levels across the body of the gene when the plants were returned to warm conditions [9]. The model predicted that the quantitative nature of vernalization would be achieved through a population average, with longer exposure to cold leading to a higher proportion of cells in which *FLC* loci have digitally switched to the fully silenced M state. This prediction was validated through analysis of an *FLC*-GUS fusion in *Arabidopsis* plants [2].

A further, fundamental prediction of the model was the existence of an opposing state to the stably repressed M state. This opposing A state would be likely to involve a histone modification associated with active gene expression—in *S. pombe*, the opposing modifications were thought to be acetylation/methylation of the same residue on the histone tail [4]. We therefore systematically screened the dynamic behavior of a series of histone modifications at *FLC* before, during, and after cold exposure and compared them with the H3K27me3 profile. Higher-resolution ChIP analysis (compared to our previous analysis) was used on material showing quantitative epigenetic silencing of *FLC* expression (Figure S1A available online) [2, 10]. A basal level of H3K27me3 was found across *FLC*, consistent with the low levels of PRC2 before cold exposure [9], with a slight peak at the nucleation region just downstream of the transcription start site (TSS) (Figure 1A and Table S1). During the cold, H3K27me3 levels accumulated quantitatively at the nucleation region, saturating after 6 weeks of cold (Figure 1A), consistent with the PHD-PRC2 complex accumulating at the same region during cold exposure [9]. At 8 weeks of cold exposure, the H3K27me3 began to spread slightly across the locus, but this spreading predominantly occurred after plants were transferred back to warm conditions for 7 days [11] (Figure 1B).

The model predicts that the A state modification should show a mirror image of the H3K27me3 profile at *FLC*, with high levels before vernalization across the whole *FLC* gene [2]. Genome-wide analysis in many organisms has suggested H3K36me3 and H3K36me2 generally accumulate to high levels in gene bodies through linkage with productive transcription [12–14]. We therefore analyzed the profiles of H3K36me2 and H3K36me3 at *FLC*. H3K36me2 accumulation was very low before cold, comparable to the negative control (Figure S1B), and did not obviously change in plants given cold treatment (Figure S1C). However, the H3K36me3 profile across *FLC* was rather different, with a strong peak at the nucleation region and somewhat elevated levels across the gene body before cold (Figure 1C). The H3K36me3 accumulation at the nucleation region was gradually suppressed with increasing

*Correspondence: caroline.dean@jic.ac.uk

This is an open access article under the CC BY license (<http://creativecommons.org/licenses/by/3.0/>).



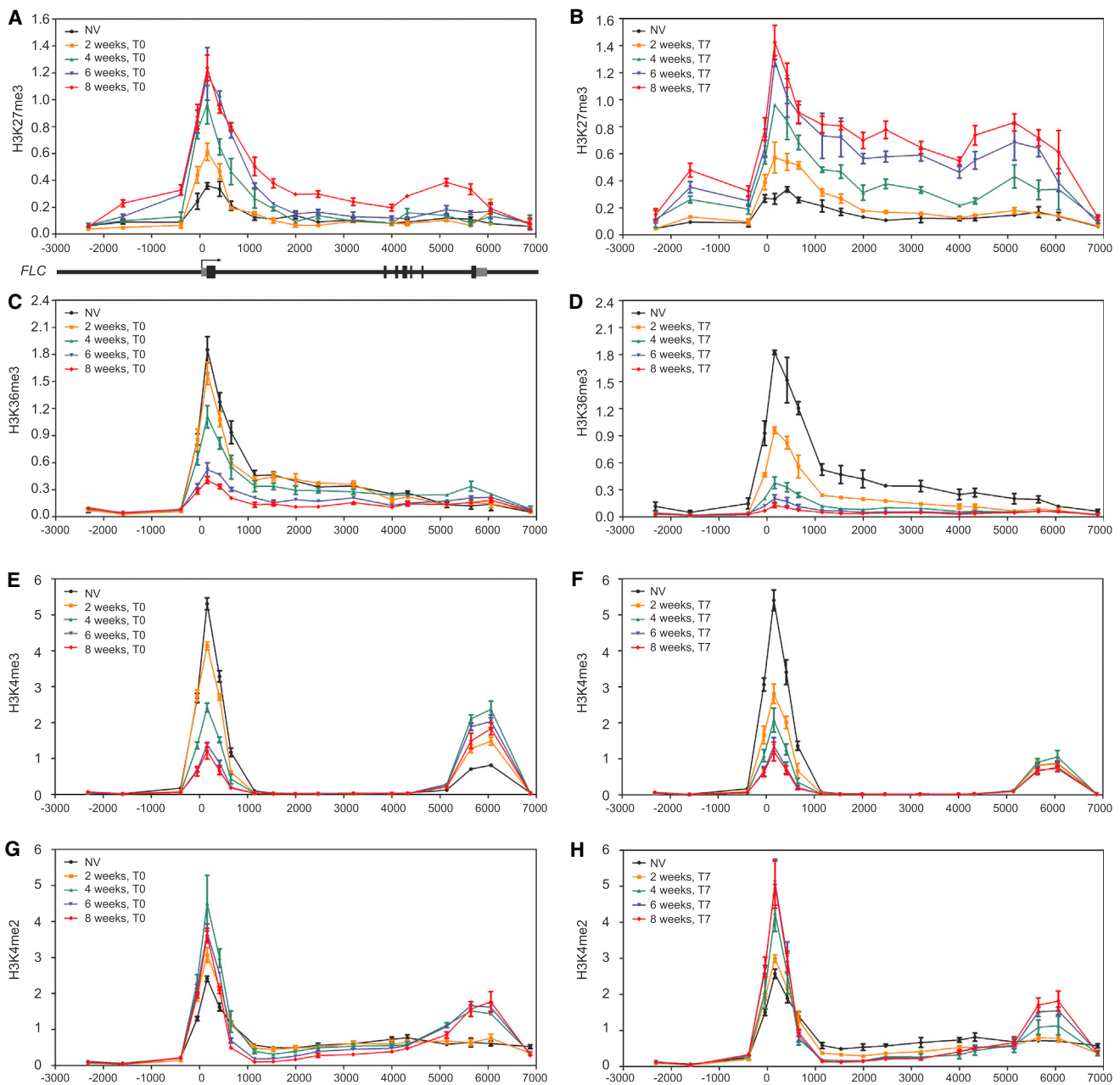


Figure 1. Histone Modifications at FLC during Vernalization

(A, C, E, and G) H3K27me3 (A), H3K36me3 (C), H3K4me3 (E), and H3K4me2 (G) profiles across the *FLC* locus for nonvernalized plants (NV) and after different lengths (2, 4, 6, and 8 weeks) of cold treatment, without postcold growth (T0). *FLC* gene structure is shown schematically at the bottom of (A).

(B, D, F, and H) H3K27me3 (B), H3K36me3 (D), H3K4me3 (F), and H3K4me2 (H) profiles across *FLC* locus for nonvernalized plants and after different lengths (2, 4, 6, and 8 weeks) of cold treatment, with 7 days postcold growth (T7). Data were presented as the ratio of (*FLC*/H3) to (reference gene/H3). *STM* was used as the reference gene for H3K27me3 and *ACT1N* was used for H3K36me3, H3K4me3 and H3K4me2.

Values represent the average and SEM of three independent biological replicates in all cases. See also [Figure S1](#) and [Table S1](#).

cold. The reduction between 2 and 6 weeks of cold was strongest and coincided with the largest increases in H3K27me3 in the nucleation region. H3K36me3 outside the nucleation region also decreased, such that after 6 weeks of cold H3K36me3 levels in the gene body were very low (Figure 1C). The H3K36me3 profile that we observed at *FLC* was distinct from some that of other organisms, and we also found similar patterns at two housekeeping genes, *ACT1N* and *UBC* (Figures S1D and S1E). Consistently, a metagenome analysis of the *A. thaliana* genome has also shown an H3K36me3 profile

over genic regions that differs from that seen in yeast and mammals [15], so H3K36me3 may play a different role in the *Arabidopsis* genome. Overall, there was a significant anticorrelation between H3K36me3 and H3K27me3 at all locations across *FLC* during the different phases of the vernalization process. The antagonism between H3K36me3 and H3K27me3 was, however, clearest at the nucleation region of *FLC* as the plants experienced an increasing duration of cold. The pattern of decreasing H3K36me3 levels as H3K27me3 increased (Figures 1A–1D) fits the opposing

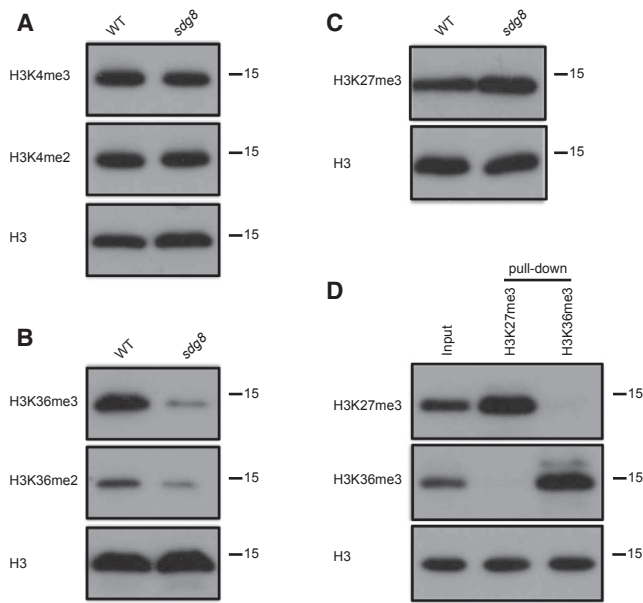


Figure 2. H3K36me3 Is Mainly Delivered by *SDG8* and Rarely Coexists with H3K27me3 on the Same Histone Tail
(A) Global levels of H3K4me3 and H3K4me2 in the wild-type (WT) and *sdg8* mutant. Antibodies used are shown on the left. Molecular weights (kDa) are indicated on the right. Histone H3 was used as the loading control.
(B) Global levels of H3K36me3 and H3K36me2 in the WT and *sdg8* mutant.
(C) Global level of H3K27me3 in the WT and *sdg8* mutant.
(D) H3K36me3 and H3K27me3 rarely coexist on the same histone tail, as shown by immunoprecipitation and western blotting. Histone H3 was used as the loading control.

pattern expected from the model. However, the relatively low H3K36me3 levels in the gene body before vernalization did not fit predictions of the model—the opposing modification was expected to be at higher levels over the gene body in order to ensure mitotic stability through many generations of cell division.

H3K4me3 and H3K4me2 are two other well-characterized histone modifications associated with gene activation [16, 17]. These two modifications have previously been shown to be important for *FLC* regulation [18–20]. Therefore, we analyzed the dynamics of H3K4me3 and H3K4me2 localization in the different regions of *FLC* at different phases of vernalization. Before cold, H3K4me3 was enriched over just two regions of *FLC*, a high peak at the nucleation region and a smaller peak at the 3' end of sense *FLC* (distal peak) (Figure 1E). The position of the latter peak corresponds to the promoter of a set of *FLC* antisense transcripts called *COOLAIR* [21]. Very little other H3K4me3 enrichment was found in the *FLC* gene body (from +1,000 to +5,000) (Figure 1E). During cold exposure, H3K4me3 levels in the nucleation region gradually decreased, reaching their lowest level after 6–8 weeks of cold (Figure 1E). As was observed for H3K36me3, H3K4me3 levels in plants given 2 and 4 weeks of cold continued to drop when the plants were transferred to the warm (Figures 1E and 1F). Interestingly, the 3' H3K4me3 peak gradually increased for the first 4 weeks of cold, then slowly came down (after 6 and 8 weeks of cold) (Figure 1E). This coincides with the increase in *COOLAIR* transcription during the first few weeks of cold exposure [21]. After transfer back to the warm, the distal peak of H3K4me3 returned to precold levels (Figure 1F), again coinciding with low levels of *COOLAIR* transcription. Thus,

H3K4me3 and H3K27me3 dynamics showed opposing dynamics at the nucleation region, but this did not extend to the gene body, where H3K4me3 levels were extremely low, or to the 3' end of *FLC*, over the *COOLAIR* promoter. Hence, H3K4me3 does not have the characteristics that suggest that it functions as an opposing mark to H3K27me3 at *FLC*. In mouse and human embryonic stem cells, a large number of PRC2 targets were covered by bivalent domains with H3K4me3 and H3K27me3, but few were modified by H3K36me3 [22, 23]. This implies that, in general, H3K4me3 is unlikely to be the opposing mark to H3K27me3.

The dynamics of H3K4me2 were also measured over *FLC* during vernalization. Before cold exposure, H3K4me2 was enriched over the whole locus, with the highest levels at the nucleation region and lowest levels in the gene body and 3' end of *FLC* (Figure 1G). During the cold, H3K4me2 dynamics showed distinct behaviors in the different *FLC* regions. At the nucleation region, H3K4me2 accumulated for the first 4 weeks of cold, and then decreased slightly. Within the gene body, H3K4me2 gradually decreased during the cold and a small 3' peak developed over the *COOLAIR* promoter, but only after 4 weeks, and then did not increase any further (Figure 1G). The increased level of H3K4me2 at the nucleation region after 2 and 4 weeks of cold was stable after transfer back to the warm. However, after return to the warm after 6 and 8 weeks of cold exposure, H3K4me2 levels increased further. In the *FLC* gene body, there was a small reduction of H3K4me2 after return to the warm, with the largest peak in the 3' region at the *COOLAIR* promoter, where we observed different dynamics as compared to H3K4me3 (Figure 1H). Overall, these dynamics show that H3K4me2 is also unlikely to act as the opposing modification to H3K27me3 during the switch of expression states in vernalization.

None of the H3K36me3, H3K36me2, H3K4me3, and H3K4me2 modifications analyzed exactly fitted the theoretically predicted pattern for the opposing modification to H3K27me3 at *FLC* during all phases of the vernalization process. However, H3K36me3 fitted most closely over both the nucleation region and gene body, although levels over the gene body were lower than predicted prior to the cold. To further verify the predicted functional antagonism between H3K36me3 and H3K27me3, we assayed H3K27me3 levels in genotypes deficient in H3K36me3. *SDG8* has recently been shown to be the specific methyltransferase for H3K36 at *FLC* [24], despite previous confusion over whether *SDG8* methylated H3K36 and H3K4 [25–28]. We extended this finding to show that global levels of H3K4me3 and H3K4me2 were unchanged in the *Arabidopsis sdg8* mutant (Figure 2A), but H3K36me3 and H3K36me2 decreased significantly (Figure 2B). Our data therefore implicate *SDG8* as the major H3K36me3 methyltransferase in the *Arabidopsis thaliana* genome. Importantly, western blots suggest that global levels of H3K27me3 are also increased in *sdg8* (Figure 2C), suggesting that H3K36 methylation antagonizes H3K27me3 in a genome-wide manner.

Considering this antagonism between H3K36me3 and H3K27me3, we asked whether the two modifications could colocalize on the same histone tail in *Arabidopsis thaliana*. Analysis of nucleosomes in mouse embryonic stem cells, mouse embryonic fibroblasts, and HeLa cells has shown H3K27me2/H3K27me3 occurs both asymmetrically and symmetrically, i.e., on one or both histone tails of each nucleosome [29, 30]. Bivalent nucleosomes carry H3K4me3 or H3K36me3 along with H3K27me3 on opposite H3 tails and resolve to

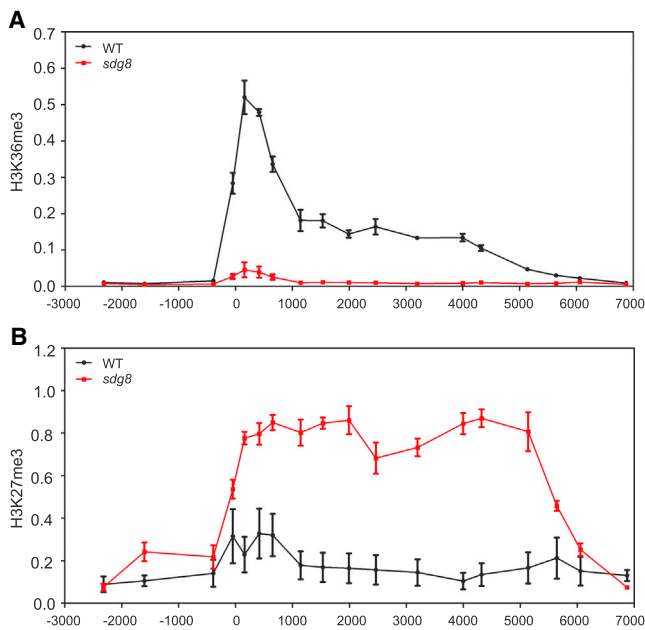


Figure 3. *FLC* Is in a Fully Silenced State in the *sdg8* Mutant
(A) H3K36me3 levels at *FLC* in an *sdg8* mutant relative to H3 (H3K36me3 *FLC*/H3 *FLC*).
(B) H3K27me3 pattern at *FLC* in an *sdg8* mutant.
Data are shown as the ratio of H3K27me3 *FLC*/H3 *FLC* to H3K27me3 *STM*/H3 *STM*. Seedlings were harvested in nonvernalized conditions. Values represent the average and SEM of three independent biological replicates. See also [Figure S2](#).

either one or other modification states during differentiation [29]. We extracted histones from disrupted nucleosomes and enriched the H3K27me3 fraction using an anti-H3K27me3 antibody. Strikingly, H3K36me3 was hardly detected in the enriched H3K27me3 histone fraction (Figure 2D) [31]. Conversely, H3K27me3 was excluded from an enriched H3K36me3 histone fraction (Figure 2D). These data show H3K36me3 and H3K27me3 rarely coexist on the same histone H3 tail, which is consistent with the model prediction of exclusive M and A modifications. We then focused on the antagonistic dynamics of H3K36me3 and H3K27me3 at *FLC*. We measured H3K36me3 and H3K27me3 levels at *FLC* in an *sdg8* mutant. As global levels of H3K36me3 are affected by *sdg8*, it is difficult to find a good reference gene for the ChIP experiments (Figure S2A), so we normalized all H3K36me3 data to H3 directly. For H3K27me3, no significant difference was found at *STM* between the wild-type and the *sdg8* mutant (Figure S2B), so *STM* was used as the reference gene. Consistent with the large reduction in H3K36me3 globally, we found a large decrease in H3K36me3 at *FLC* in *sdg8* (Figure 3A) and a correspondingly large increase in H3K27me3 (Figure 3B), similar in extent to the fully vernalized state (seen at 8 weeks of cold followed by 7 days of warm; Figure 1B). *FLC* expression analysis shows that *FLC* is fully silenced in *sdg8* (Figure S2C), so loss of an H3K36 methyltransferase leads to a reduction of H3K36me3 at *FLC* and upregulation of H3K27me3. This finding is again in agreement with our earlier modeling, in which loss of the activating A mark (H3K36me3) would lead to M modifications (H3K27me3) spreading across the entire locus, with associated epigenetic silencing.

The high-resolution temporal and spatial analysis shown here has now provided a clear picture of the dynamics of a

series of histone modifications at the *FLC* locus during the phases of vernalization. The intent was to discover a modification with a pattern that was a mirror to that of H3K27me3, known to be centrally important in the Polycomb-induced silencing mechanism [2]. None of the profiles of the active histone modifications exactly fitted the mirror pattern for the opposing epigenetic state predicted from earlier modeling. However, similar to model predictions, a clear antagonism was discovered between H3K36me3 and H3K27me3, both for the nucleation region and the gene body. In particular, the two modifications were unable to coexist on the same histone H3 tail, and suppression of H3K36me3 (*sdg8* mutant) led to H3K27me3 upregulation. Furthermore, in the nucleation region, the quantitative decrease in H3K36me3 and mirror-like quantitative increase in H3K27me3 suggest that they are indeed markers of opposing states that switch with increasing cold exposure.

However, outside of the nucleation region, a mirror-like opposition of states between H3K36me3 and H3K27me3 applied less well. Importantly, H3K36me3 was only present at relatively low levels across the gene body prior to cold exposure, in contrast to the high levels predicted by modeling. Potentially, epigenetic memory could be written only in the nucleation region, where mirror H3K36me3/H3K27me3 states do exist. However, this interpretation is problematic due to the relatively small number of nucleosomes (approximately three, so approximately six histone 3 molecules) in the nucleation region. Complete loss of epigenetic marks in this limited region, either at DNA replication or simply through nucleosome swap-outs, is likely to occur with comparatively high frequency, leading to epigenetic memory loss. Hence, it is unlikely that a purely histone-based feedback mechanism could confer epigenetic memory between cell divisions based only on this limited region. Moreover, a similar conclusion is reached on consideration of the lack of a mirror image of the modifications from the low levels of H3K36me3 outside the nucleation region before cold. Accordingly, our earlier models of the vernalization process will need to be updated to reflect this analysis, with H3K36me3/H3K27me3 dynamics being necessary, but not sufficient, for epigenetic switching and memory. Additional mechanisms, potentially involving *trans*-factors, noncoding RNAs, other histone modifications, or proteins that remain bound to DNA through its replication, could encode the robust positive feedback required to enforce epigenetic inheritance of active or repressed states [1].

The dynamics during cold exposure at *FLC* and the genome-wide antagonism between H3K36me3 and H3K27me3 suggest a close functional connection between the complexes delivering H3K36me3 and H3K27me3. The activity of H3K36 methyltransferase has been shown to inhibit the enzyme activity of the PRC2 H3K27me3 complex [29, 30, 32]. This mutual inhibition is again similar to interactions predicted from our earlier modeling, in which each histone mark was assumed to recruit factors that not only reinforced the presence of that mark, but that also inhibited the opposing mark. Moreover, a similar feature extends to the PRC2 complex, which also contains associated proteins that recognize H3K36me3 and recruit H3K36 demethylase to facilitate its activity [23, 33–35].

An interesting open question for the future is whether the gradual change from H3K36me3 to H3K27me3 observed at the nucleation region during cold exposure involves progressive, gradual changes in modification levels of the different histone tails in all cells. An alternative to this “analog” mechanism would be a full “digital” switch from an H3K36me3 to

H3K27me3 nucleation peak in an increasing proportion of cells as the duration of cold exposure increases [36]. The latter digital scenario has been found for the spreading of the silencing modifications across the body of the gene after transfer back to the warm [2]. Regardless of the mechanism, the opposing dynamics of H3K36me3 and H3K27me3 in the nucleation region are clearly tightly regulated by temperature. We therefore propose that this balance is used by plants to “register” the duration of cold exposure at the *FLC* locus.

Supplemental Information

Supplemental Information includes Supplemental Experimental Procedures and two figures and table can be found with this article online at <http://dx.doi.org/10.1016/j.cub.2014.06.047>.

Acknowledgments

We thank Yoo-Sun Noh for providing *FRI sdg8* seeds and members of the C.D. group for useful discussions. The work was supported by a European Research Council grant (233039 ENVGENE).

Received: April 26, 2014

Revised: June 2, 2014

Accepted: June 17, 2014

Published: July 24, 2014

References

1. Moazed, D. (2011). Mechanisms for the inheritance of chromatin states. *Cell* 146, 510–518.
2. Angel, A., Song, J., Dean, C., and Howard, M. (2011). A Polycomb-based switch underlying quantitative epigenetic memory. *Nature* 476, 105–108.
3. Margueron, R., and Reinberg, D. (2010). Chromatin structure and the inheritance of epigenetic information. *Nat. Rev. Genet.* 11, 285–296.
4. Dodd, I.B., Micheelsen, M.A., Sneppen, K., and Thon, G. (2007). Theoretical analysis of epigenetic cell memory by nucleosome modification. *Cell* 129, 813–822.
5. Sneppen, K., and Dodd, I.B. (2012). A simple histone code opens many paths to epigenetics. *PLoS Comput. Biol.* 8, e1002643.
6. Gendall, A.R., Levy, Y.Y., Wilson, A., and Dean, C. (2001). The *VERNALIZATION 2* gene mediates the epigenetic regulation of vernalization in *Arabidopsis*. *Cell* 107, 525–535.
7. Greb, T., Mylne, J.S., Crevillen, P., Geraldo, N., An, H., Gendall, A.R., and Dean, C. (2007). The PHD finger protein *VRN5* functions in the epigenetic silencing of *Arabidopsis FLC*. *Curr. Biol.* 17, 73–78.
8. Sung, S., and Amasino, R.M. (2004). Vernalization in *Arabidopsis thaliana* is mediated by the PHD finger protein *VIN3*. *Nature* 427, 159–164.
9. De Lucia, F., Crevillen, P., Jones, A.M., Greb, T., and Dean, C. (2008). A PHD-polycomb repressive complex 2 triggers the epigenetic silencing of *FLC* during vernalization. *Proc. Natl. Acad. Sci. USA* 105, 16831–16836.
10. Bastow, R., Mylne, J.S., Lister, C., Lippman, Z., Martienssen, R.A., and Dean, C. (2004). Vernalization requires epigenetic silencing of *FLC* by histone methylation. *Nature* 427, 164–167.
11. Finnegan, E.J., and Dennis, E.S. (2007). Vernalization-induced trimethylation of histone H3 lysine 27 at *FLC* is not maintained in mitotically quiescent cells. *Curr. Biol.* 17, 1978–1983.
12. Vakoc, C.R., Sachdeva, M.M., Wang, H., and Blobel, G.A. (2006). Profile of histone lysine methylation across transcribed mammalian chromatin. *Mol. Cell. Biol.* 26, 9185–9195.
13. Smolle, M., Venkatesh, S., Gogol, M.M., Li, H., Zhang, Y., Florens, L., Washburn, M.P., and Workman, J.L. (2012). Chromatin remodelers *lsw1* and *Chd1* maintain chromatin structure during transcription by preventing histone exchange. *Nat. Struct. Mol. Biol.* 19, 884–892.
14. Le Martelot, G., Canella, D., Symul, L., Migliavacca, E., Gilardi, F., Liechti, R., Martin, O., Harshman, K., Delorenzi, M., Desvergne, B., et al.; CycLiX Consortium (2012). Genome-wide RNA polymerase II profiles and RNA accumulation reveal kinetics of transcription and associated epigenetic changes during diurnal cycles. *PLoS Biol.* 10, e1001442.
15. Roudier, F., Ahmed, I., Bérard, C., Sarazin, A., Mary-Huard, T., Cortijo, S., Bouyer, D., Caillieux, E., Duvernois-Berthet, E., Al-Shikhey, L., et al. (2011). Integrative epigenomic mapping defines four main chromatin states in *Arabidopsis*. *EMBO J.* 30, 1928–1938.
16. Eissenberg, J.C., and Shilatifard, A. (2010). Histone H3 lysine 4 (H3K4) methylation in development and differentiation. *Dev. Biol.* 339, 240–249.
17. Ruthenburg, A.J., Allis, C.D., and Wysocka, J. (2007). Methylation of lysine 4 on histone H3: intricacy of writing and reading a single epigenetic mark. *Mol. Cell* 25, 15–30.
18. Saleh, A., Alvarez-Venegas, R., and Avramova, Z. (2008). Dynamic and stable histone H3 methylation patterns at the *Arabidopsis FLC* and *AP1* loci. *Gene* 423, 43–47.
19. Pien, S., Fleury, D., Mylne, J.S., Crevillen, P., Inzé, D., Avramova, Z., Dean, C., and Grossniklaus, U. (2008). *ARABIDOPSIS TRITHORAX1* dynamically regulates *FLOWERING LOCUS C* activation via histone 3 lysine 4 trimethylation. *Plant Cell* 20, 580–588.
20. Liu, F., Quesada, V., Crevillén, P., Bäurle, I., Swiezewski, S., and Dean, C. (2007). The *Arabidopsis* RNA-binding protein *FCA* requires a lysine-specific demethylase 1 homolog to downregulate *FLC*. *Mol. Cell* 28, 398–407.
21. Swiezewski, S., Liu, F., Magusin, A., and Dean, C. (2009). Cold-induced silencing by long antisense transcripts of an *Arabidopsis* Polycomb target. *Nature* 462, 799–802.
22. Ku, M., Koche, R.P., Rheinbay, E., Mendenhall, E.M., Endoh, M., Mikkelsen, T.S., Presser, A., Nusbaum, C., Xie, X., Chi, A.S., et al. (2008). Genomewide analysis of PRC1 and PRC2 occupancy identifies two classes of bivalent domains. *PLoS Genet.* 4, e1000242.
23. Brien, G.L., Gambero, G., O’Connell, D.J., Jerman, E., Turner, S.A., Egan, C.M., Dunne, E.J., Jurgens, M.C., Wynne, K., Piao, L., et al. (2012). Polycomb PHF19 binds H3K36me3 and recruits PRC2 and demethylase NO66 to embryonic stem cell genes during differentiation. *Nat. Struct. Mol. Biol.* 19, 1273–1281.
24. Shafiq, S., Berr, A., and Shen, W.H. (2014). Combinatorial functions of diverse histone methylations in *Arabidopsis thaliana* flowering time regulation. *New Phytol.* 201, 312–322.
25. Rao, B., Shibata, Y., Strahl, B.D., and Lieb, J.D. (2005). Dimethylation of histone H3 at lysine 36 demarcates regulatory and nonregulatory chromatin genome-wide. *Mol. Cell. Biol.* 25, 9447–9459.
26. Zhao, Z., Yu, Y., Meyer, D., Wu, C., and Shen, W.H. (2005). Prevention of early flowering by expression of *FLOWERING LOCUS C* requires methylation of histone H3 K36. *Nat. Cell Biol.* 7, 1256–1260.
27. Ko, J.H., Mitina, I., Tamada, Y., Hyun, Y., Choi, Y., Amasino, R.M., Noh, B., and Noh, Y.S. (2010). Growth habit determination by the balance of histone methylation activities in *Arabidopsis*. *EMBO J.* 29, 3208–3215.
28. Tang, X., Lim, M.H., Pelletier, J., Tang, M., Nguyen, V., Keller, W.A., Tsang, E.W., Wang, A., Rothstein, S.J., Harada, J.J., and Cui, Y. (2012). Synergistic repression of the embryonic programme by *SET DOMAIN GROUP 8* and *EMBRYONIC FLOWER 2* in *Arabidopsis* seedlings. *J. Exp. Bot.* 63, 1391–1404.
29. Voigt, P., LeRoy, G., Drury, W.J., 3rd, Zee, B.M., Son, J., Beck, D.B., Young, N.L., Garcia, B.A., and Reinberg, D. (2012). Asymmetrically modified nucleosomes. *Cell* 151, 181–193.
30. Yuan, W., Xu, M., Huang, C., Liu, N., Chen, S., and Zhu, B. (2011). H3K36 methylation antagonizes PRC2-mediated H3K27 methylation. *J. Biol. Chem.* 286, 7983–7989.
31. Johnson, L., Mollah, S., Garcia, B.A., Muratore, T.L., Shabanowitz, J., Hunt, D.F., and Jacobsen, S.E. (2004). Mass spectrometry analysis of *Arabidopsis* histone H3 reveals distinct combinations of post-translational modifications. *Nucleic Acids Res.* 32, 6511–6518.
32. Schmitges, F.W., Prusty, A.B., Faty, M., Stützer, A., Lingaraju, G.M., Aiwazian, J., Sack, R., Hess, D., Li, L., Zhou, S., et al. (2011). Histone methylation by PRC2 is inhibited by active chromatin marks. *Mol. Cell* 42, 330–341.
33. Cai, L., Rothbart, S.B., Lu, R., Xu, B., Chen, W.Y., Tripathy, A., Rockowitz, S., Zheng, D., Patel, D.J., Allis, C.D., et al. (2013). An H3K36 methylation-engaging Tudor motif of polycomb-like proteins mediates PRC2 complex targeting. *Mol. Cell* 49, 571–582.
34. Musselman, C.A., Gibson, M.D., Hartwick, E.W., North, J.A., Gatchalian, J., Poirier, M.G., and Kutateladze, T.G. (2013). Binding of PHF1 Tudor to H3K36me3 enhances nucleosome accessibility. *Nat. Commun.* 4, 2969.
35. Ballaré, C., Lange, M., Lapinaite, A., Martin, G.M., Morey, L., Pascual, G., Liefke, R., Simon, B., Shi, Y., Gozani, O., et al. (2012). Phf19 links methylated Lys36 of histone H3 to regulation of Polycomb activity. *Nat. Struct. Mol. Biol.* 19, 1257–1265.
36. Voigt, P., Tee, W.W., and Reinberg, D. (2013). A double take on bivalent promoters. *Genes Dev.* 27, 1318–1338.

Current Biology, Volume 24

Supplemental Information

**Antagonistic Roles for H3K36me3
and H3K27me3 in the Cold-Induced
Epigenetic Switch at *Arabidopsis FLC***

Hongchun Yang, Martin Howard, and Caroline Dean

Supplemental information

Supplemental Figures and Legends

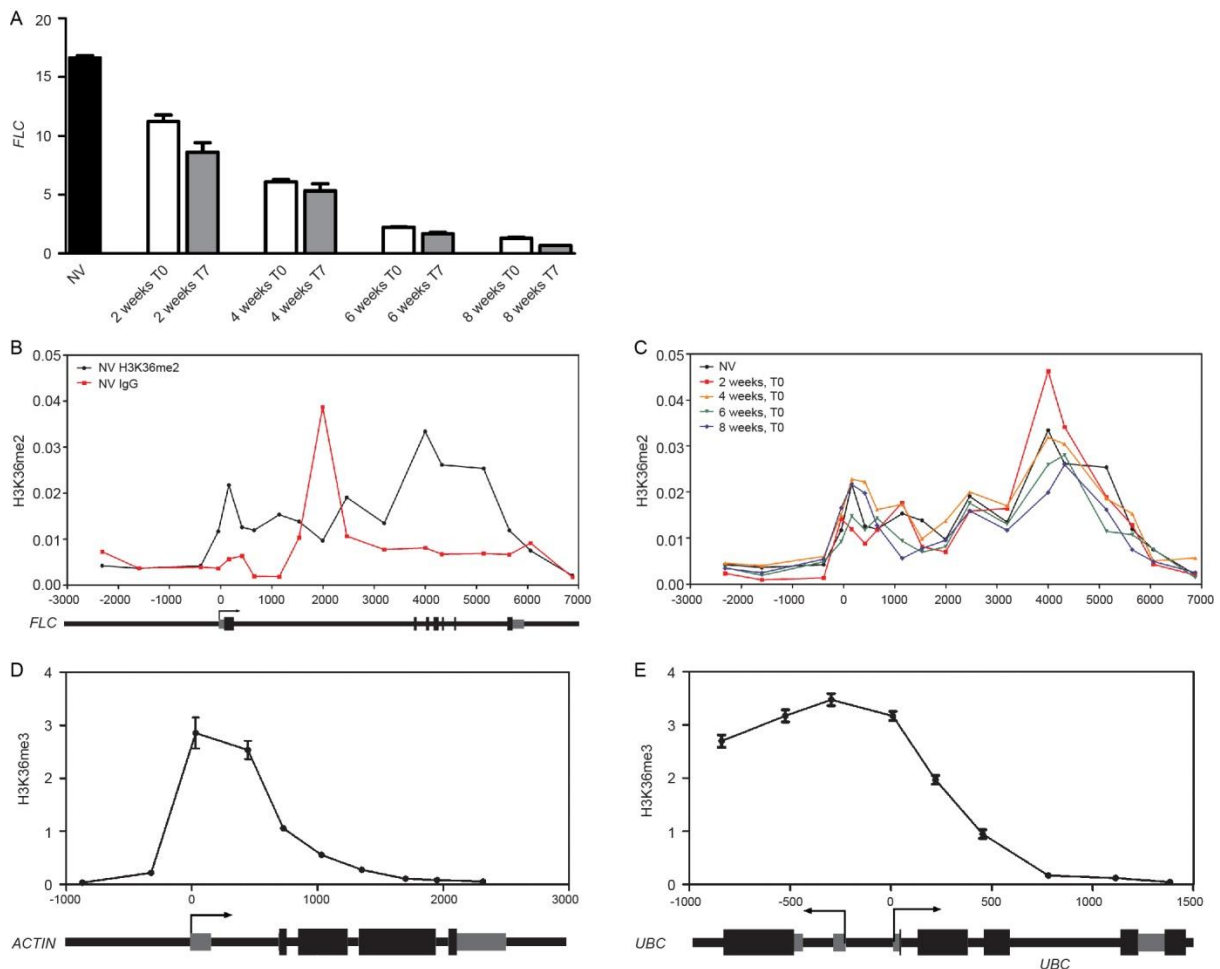


Figure S1, related to Figure 1. Characterization of chromatin modifications at *FLC*, *ACTIN* and *UBC*.

(A) *FLC* silencing in the plant material used in the ChIP experiments. The materials were harvested after the indicated treatments. Levels are relative to *UBC*. Values represent the average and SEM of three independent biological replicates.

(B) H3K36me2 levels for non-vernalized plants. The IgG ChIP was used as a negative control. Values are relative to H3 (H3K36me2 or IgG *FLC*/H3 *FLC*).

(C) Levels of H3K36me2 at *FLC* for non-vernalized plants (NV) and after 2, 4, 6 and 8 weeks of cold treatment, without post-cold growth (T0), respectively.

Values represent as H3K36me2 *FLC*/H3 *FLC* in (B) and (C).

(D) and (E) H3K36me3 patterns at *ACTIN* (D) and *UBC* (E). The schematic gene structures of *ACTIN* and *UBC* are shown. 0 is relative to transcription start site. Data were relative to H3 (H3K36me3 *ACTIN* /H3 *ACTIN* or H3K36me3*UBC*/ H3 *UBC*). Data shown are average and SEM from 3 independent biological replicates.

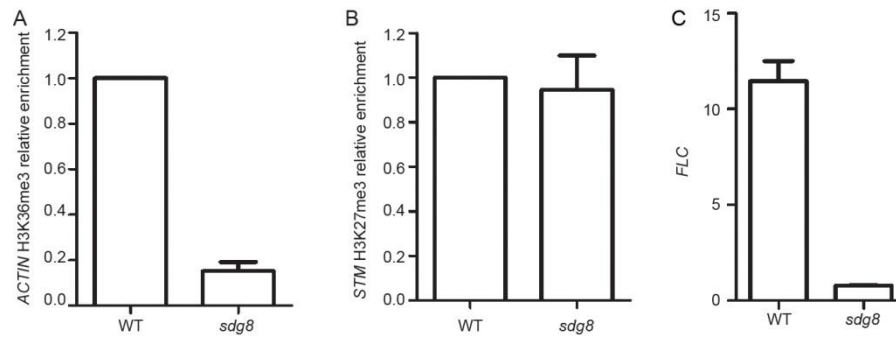


Figure S2, related to Figure 3. Characterization of *sdg8* mutant.

(A) Relative H3K36me3 levels at *ACTIN* in WT and *sdg8* mutant.

(B) Relative H3K27me3 levels at *STM* in WT and *sdg8* mutant.

Data in (A) and (B) represent the average and SEM of three independent biological replicates.

(C) *FLC* expression in *sdg8* mutant in NV conditions. *FLC* mRNA expression was determined relative to *UBC*. Values represent the average and SEM of three independent biological replicates.

Supplemental Experimental Procedures

Plant material and growth conditions

All plants used are in the *Columbia FRI sf2* background and described previously [S1]. *sdg8* was described previously [S2]. Plant growth conditions were described previously [S1]. T0 seedlings were harvested immediately after the indicated cold treatments in a cold room. T7 seedlings were grown for 7 days after transfer back to warm conditions.

ChIP and Q-PCR

Nuclei were extracted using Honda buffer as described previously [S3]. The sonication, immunoprecipitation, DNA recovery and purification were performed as previously described [S1]. The antibodies used were: anti-H3 (Abcam, ab1791), anti-H3K27me3 (Millipore, 07-449), anti-H3K36me2 (Millipore, 07-369), anti-H3K36me3 (Abcam, ab9050), anti-H3K4me3 (Millipore, 04-745), anti-H3K4me2 (Millipore, 07-030) and normal rabbit IgG (Millipore, PP64). All ChIP data were quantified by quantitative real-time PCR (Q-PCR). Values represent the average and SEM of three independent biological replicates in all cases. *FLC* expression was determined relative to *UBC*.

Western blots and immunoprecipitation

Nuclei were prepared using Honda buffer. The nuclei pellet was suspended in nuclei lysis buffer (50 mM Tris-HCl pH8.0, 10 mM EDTA pH8.0, 1% SDS, cocktail). After extreme sonication, the lysis was centrifuged at 12,000 rpm for 10 min. The supernatant was collected as the histone extract for western blots and immunoprecipitation. For immunoprecipitation, the histone extract was diluted 10 times by dilution buffer (1.1% Triton X-100, 1.2 mM EDTA pH8.0, 16.7 mM Tris-HCl pH8.0, 167 mM NaCl), then incubated with anti-H3K27me3 or anti-H3K36me3 for 3 h at 4 °C and captured by the Dynabeads protein-A (Invitrogen 10002D). The beads were washed 4 times with washing buffer (50 mM Tris-HCl

pH8.0, 2 mM EDTA pH8.0, 1% Triton X-100, 0.1% SDS, 200 mM NaCl). The immunoprecipitated histones were eluted with SDS-PAGE loading buffer.

Supplemental Reference

- S1. Angel, A., Song, J., Dean, C., and Howard, M. (2011). A Polycomb-based switch underlying quantitative epigenetic memory. *Nature* *476*, 105-108.
- S2. Ko, J.H., Mitina, I., Tamada, Y., Hyun, Y., Choi, Y., Amasino, R.M., Noh, B., and Noh, Y.S. (2010). Growth habit determination by the balance of histone methylation activities in *Arabidopsis*. *EMBO J* *29*, 3208-3215.
- S3. Sun, Q., Csorba, T., Skourti-Stathaki, K., Proudfoot, N.J., and Dean, C. (2013). R-loop stabilization represses antisense transcription at the *Arabidopsis* FLC locus. *Science* *340*, 619-621.